19

Unmixing Based Landsat ETM+ and ASTER Image Fusion for Hybrid Multispectral Image Analysis

Nouha Mezned[1], Sâadi Abdeljaoued[1]
and Mohamed Rached Boussema[2]
[1] *Faculté des Sciences de Tunis,*
[2] *Ecole Nationale d'Ingénieurs de Tunis*
TUNISIA

1. Introduction

Monitoring the environmental risks associated with mine tailings in a quick and timely fashion is the first step towards mitigating their impact. Mine tailings may have a widespread geographical distribution; their location and extent may also vary along time, due to reprocessing and disposal activities. For these reasons, the characterization of mine tailings using traditional field work alone is both costly and inefficient. Remote sensing techniques have been proven extremely valuable in the inventory, characterization, and remediation of mine tailings elsewhere (Peters & Hauff, 2000). Determining the location, extent, and geochemistry of mine tailings is the first step towards remediation and hence avoidance of negative health and environmental consequences.

In this chapter we focus on mine tailing cartography and monitoring using multispectral data (Landsat ETM+ and ASTER). These data are well available from much passed years at regular intervals. We are particularly interest in the case study of zinc and lead mines in the north of Tunisia (North Africa). Particularly, the mine of Jebel (Hill) Hallouf-Bouaouane (36°42'N 9°0'5''E), which is forsaken since 1986, is among several types of mines in the Mejerda river watershed (Mansouri, 1980). The Mejerda River is the most important river which is exploited for the agriculture irrigation and drinking water alimentation of the north of Tunisia. In this site, mine tailings cause the environment degradation, so it had polluted soils, vegetation and water quality (Souissi, 2007). Mine tailing cartography becomes fundamental in order to follow the environmental changes and pollution quickly.

The approach was organized in two steps; a coarse cartography based on the Landsat (Enhanced Thematic Mapper Plus) ETM+ spectral unmixing using image derived endmember and a detailed cartography based on a multispectral inter-images fusion using a simplified version of Multisensor Multiresolution Technique (MMT). The analysis of the resulting hybrid image allowed to tailing cartography refinement. Detailed fraction maps were generated.

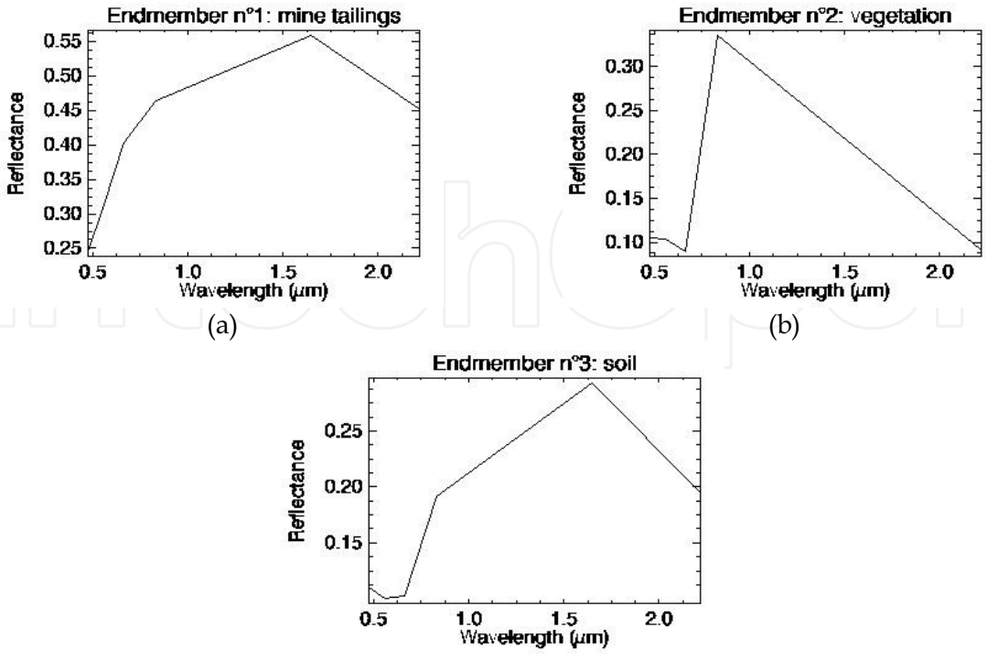

Fig. 1. The three endmember spectra selected from first three PC analyses.

The chapter is structured as follows. Section 2 is a tailing cartography approach description. In section 3, we consider a coarse and refinement cartography of the mine tailings using hybrid Multispectral data and demonstrate that its important special case. In section 4, we present results and discussion. Section 5 concludes the chapter.

2. Mine tailing cartography

The adopted cartography approach includes two main parts: The first one deal with the classification of the ETM+ data which results give the distribution and the abundance image of mine tailing surface cover. The resulting map represents a coarse mine tailing cartography. The second part, focus on the ETM+ and ASTER data fusion and analysis (Mezned et al., 2007). We used The (MS) and (Pan) ETM+ data acquired on May 3, 2000 and Aster Level 2B SWIR reflectance surface product acquired on June 26, 2000. The resulting hybrid image have the high spatial resolution of the (MS)/(Pan) Landsat ETM+ image (15m) and its relative high spectral resolution combined with ASTER SWIR image (10 bands).

2.1 Multispectral image classification

The first classification was performed on Landsat ETM+ MS/Pan fused image (196x196 pixels) with 6 bands using constrained spectral unmixing method. We used the Principal Component (PC) Spectral Sharpening technique to merge (MS) and (PAN) Landsat ETM+ data. Spectral information's are conserved as these two images were acquired by the same sensor. The used images were georeferenced, co-registered, topographically and

atmospherically corrected using the FLAASH (Cooley, 2002) software before performing the sharpening. Indeed, (Pan) data was only topographically corrected.

The first step of the analysis identifies the pure materials that are present in the scene. Principal Component (PC) analysis method was used for optimal endmember extraction (Boardman, 1993); (Carreiras and al., 2002). It allows one to reduce the dimensionality of the data and to know the number of endmembers present in the scene as explained in (Keshava & Mustard, 2002). Endmembers lay correctly at the corners of the triangular shaped diagram, indicating the purest pixel spectra (Boardman, 1993). Figure 1 show the three endmember, which were selected using the first three principal components (contain more than 95 % of the information), corresponding to tailings, vegetation and soil. Their identification was based on their typical spectra and their location.

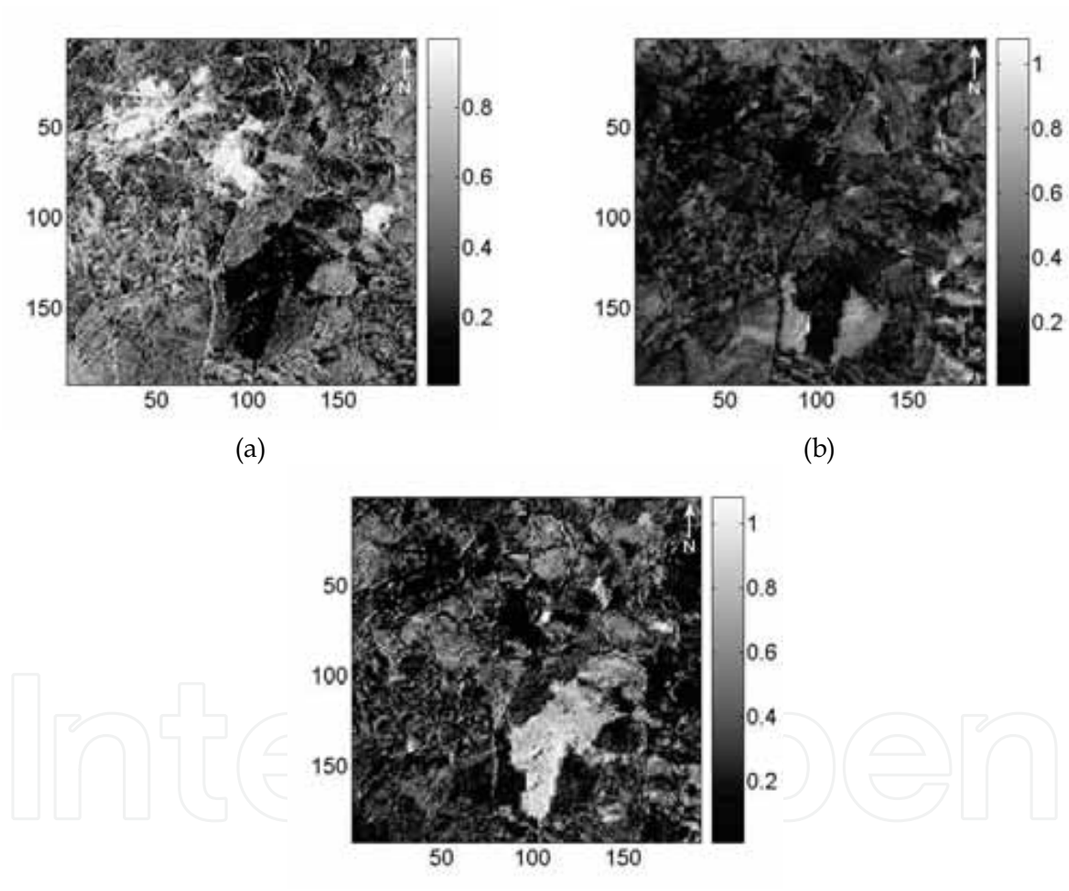

Fig. 2. Fraction maps (196x196 pixels) resulting from Landsat ETM+ coarse classification: (a) tailings, (b) vegetation and (c) soils.

The fraction maps which estimated by the constrained least-squares algorithm (Singer, 1981); (Shimabukuro & Smith, 1991) for the three pure materials are represented in Figure 2. Note that a black (respectively, white) pixel in the map indicates a large (respectively, small) value of the abundance. The accuracy of the endmember fraction maps are evaluated using

the Root Mean Square (RMS) error. The most of RMS error (96 %) are lower than 1.35 10^{-5}, which shows a good result.

2.2 Unmixing based multispectral Image Fusion

The proposed unmixing based image fusion method consists on a two data set fusion: the first set has a high spatial resolution (and low spectral resolution), called classifying instrument (CI) and the second one have a high spectral resolution (and low spatial resolution), called measuring instrument (MI). The unmixing method uses the spatial high resolution data classification (CI) to unmix the lower spatial resolution image (MI). Furthermore, the unmixing can be performed only relative to the recognized classes in the (MI) image.

The main contribution consists on considering a fusion of two different multispectral sensors. Thus, we chose the (MS) Landsat ETM+ data combined with the corresponding (PAN) band (Chavez et al., 1991) as the (CI) image (Figure 3 a) and the ASTER SWIR product as the (MI) image (Figure 3 b). These images were co-registered before fusion. The used fusion technique is based on:

- classification of the high spatial resolution image (CI). In our case, the classification of the CI Landsat ETM+ MS/Pan fused image (only 4 bands were used, the last two bands were removed due to its overlapping with the ASTER SWIR bands which represent better spectral resolution) was performed by the ISODATA unsupervised technique (Richards, 1986) with K_0 = 16 classes (gives minimal error during the constrained unmixing).
- definition of class contributions to the signal of the low spatial resolution of MI pixels. It is based on the resulting high-resolution classification map k (m, n) which represents different class areas. The contribution of class is given by the following equation:

$$c_i(l,s;k_0) = \sum_{k(m,n)\in k_0} \rho_i(l,s;m,n)$$

  where c_i (l, s; k_0) is the contribution of class k_0 to the signal of low spatial resolution of MI pixel (l, s) in different band i, and ρ_i (l, s; m, n) is a discrete approximation for the sensor PSF (Point spread function) which sum over a high resolution pixel (m, n) is assumed to be normalized to 1. The discrete PSF includes the registration component (MI image is co-registered with CI image) and the atmospheric component (CI image was corrected to eliminate the atmospheric and illumination effects before the classification and thus, these effects will be also removed during the unmixing).
- we proposed a simplified version of the constrained unmixing algorithm (Hu et al., 1999). In this algorithm, we make the hypothesis that the reflectance of MI pixels equal to the sum of the mean reflectance of each class in the window.

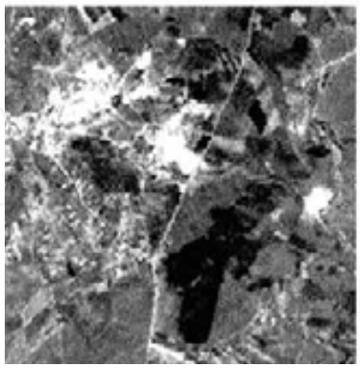

(a)

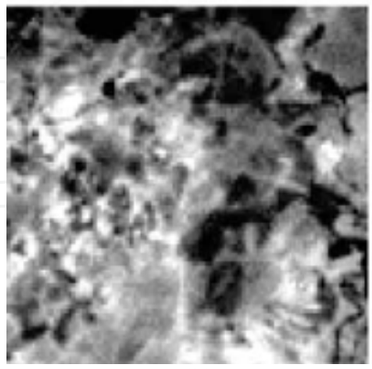

(b)

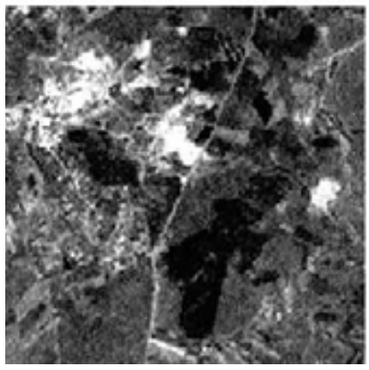

(c)

Fig. 3. Landsat ETM+ MS/Pan (196x196) with 15 m pixel size acquired in May 2000 shown in gray scale at wavelength λ=0.66 μm (a), ASTER SWIR (196x196) with 30 m pixel size acquired in June 2000 shown in gray scale at wavelength λ=2.4 μm (b) and Hybrid fused image (196x196) with 15 m pixel size shown in gray scale at wavelength λ=0.66 μm (c).

The unmixing of the MI pixels was performed in a 5 x 5 window that was moved with the step of 1 MI-pixel size. The central MI pixel in each window is unmixed by an inversion of a system of linear mixture equations that are written as following for all pixels in the window:

$$R_i(l,s) = \sum_{k=1}^{K} c_i(l,s,k)\,\bar{R}_i(k) + \varepsilon_i(l,s)$$

where R_i (l, s) is the reflectance of MI pixel (l, s) in the window, $\bar{R}_i$ (k) is the mean MI-reflectance for class k in the window and ε_i (l, s) is the model error. The numerical inversion of the linear system given in (Zhukov et al., 1999); (Zurita Milla et al., 2008) was done with the matlab software using the least-square function independently for each MI band (Matlab, 2004) This function returns the vector $\bar{R}$ that minimizes norm (C* $\bar{R}$ - R) subject to $\bar{R} \geq 0$.

- restoration of the unmixed lower resolution channels image was performed by assigning the estimated mean class reflectance to the corresponding high resolution pixels of the classification map.

The resulting hybrid image (Figure 3 c) present the high spatial resolution of the (MS)/(Pan) Landsat ETM+ image (15 m) and its relative high spectral resolution (4 bands) combined with ASTER SWIR bands (6 bands).

3. Tailing cartography refinement

The tailing cartography refinement approach includes the generation of tailing mask needed for unmixing the hybrid image. The mask was generated from the first tailing coarse cartography. It was validated before being used in the hybrid image classification process. The classification was performed using the constrained spectral unmixing method. The resulting maps represent detailed mine tailing cartography. The laboratory analyses were used as field truth for tailing maps validation.

3.1. Generation and validation of the tailing mask

The tailings fraction map represents their abundance and their spatial distribution in the study area. The mean value for tailing proportions is 0.32. This value supposes that the study area is covered by a considerable quantity of tailings. Those for vegetation and soil are estimated by 0.26 and 0.41 respectively. A tailing mask (Figure 4. a) was generated (extracted from fractional abundance map) to highlight the mine tailing area and masking the surrounding zones (vegetation and soils). The spatial distribution of the mine tailing was validated using high resolution data. The validation of tailing mask was based on aerial photo. It consists on the comparison of the tailing distribution (indicated by red lines) detected on the mask as well as aerial photo (Figure 4. c).

Indeed, certain zones are inaccessible or difficult of access. A spatial interpretation will be easier and faster. So, we refer to the interpretation of the aerial photo to analyze the distribution of the tailings in the Jebel Hallouf-Bouaouane region. The comparison reveals the presence of an individual quantity of tailings transported eastward and deposited near the Kassab wad. It is detected on the mask as well as on the aerial photo.

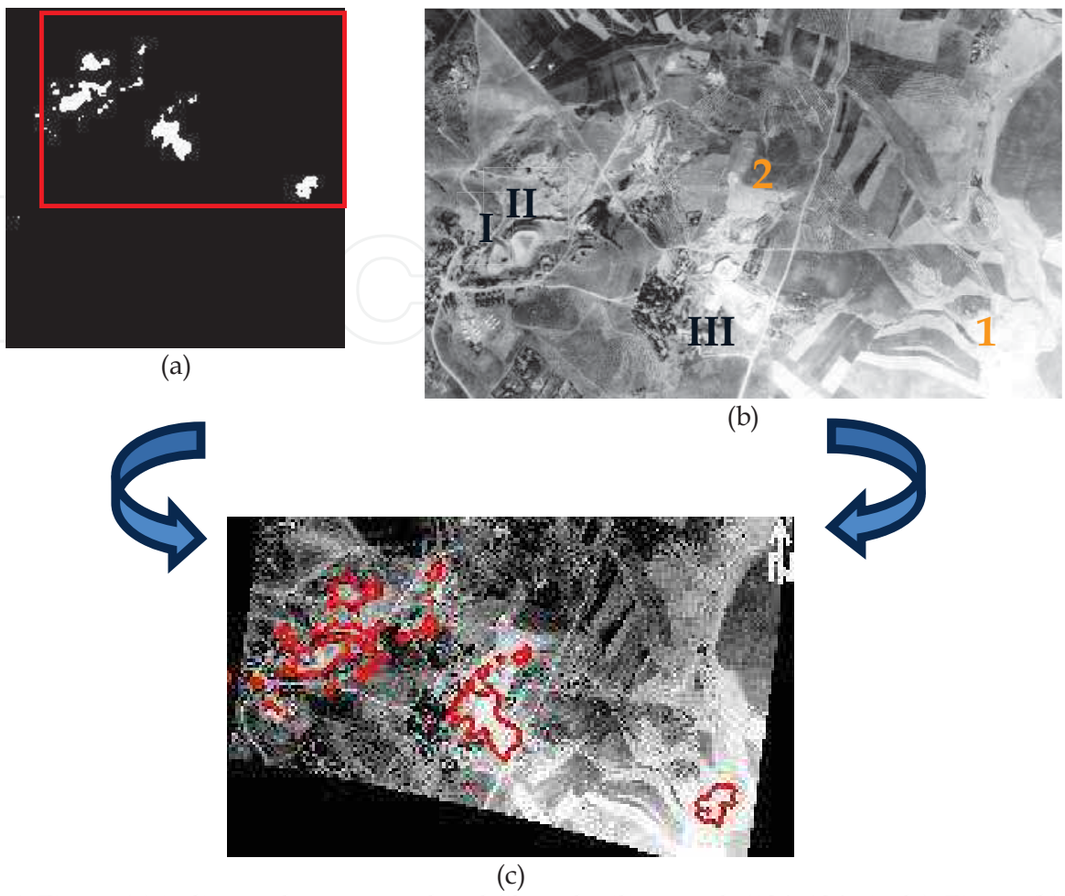

(a) (b) (c)

Fig. 4. Figure (a) indicates the generated and filtered tailing mask (196x196 pixels). Figure (b) shows the aerial photo (scale: 1/6250) scanned at 100 dpi of the corresponding Jebel Hallouf-Bouaouane region. Blue roman numbers locate tailing deposits: (I) the first dyke of Jebel Hallouf, (II) the second dyke of Jebel Hallouf and (III) the dykes of Bouaouane. Orange numbers locate the eroded and transported tailings towards: (1) kassab wad and (2) swamps in the north-east. Figure (c) shows the validation of the region of interest with 171 km^2 (indicated with red rectangle). The contours lines (red lines) which correspond to tailing zones were superposed on the georeferenced aerial photo.

3.2. Hybrid Multispectral data analysis

The classification of hybrid multispectral data, which is based on the constrained linear spectral unmixing using JPL mineral library spectra, generates mineral detailed maps. Only mine tailing pixels are used in the analysis. We used the tailing mask generated from the coarse classification to exclude the undesired zones and to analyze minerals in the tailing area.

The used endmembers are: calcite (with additionally cerusite, quartz and barite), gypsum, oxides (hematite and goethite), clays (kaolinite and illite) and pyrite. This mineralogical composition was revealed from samples by

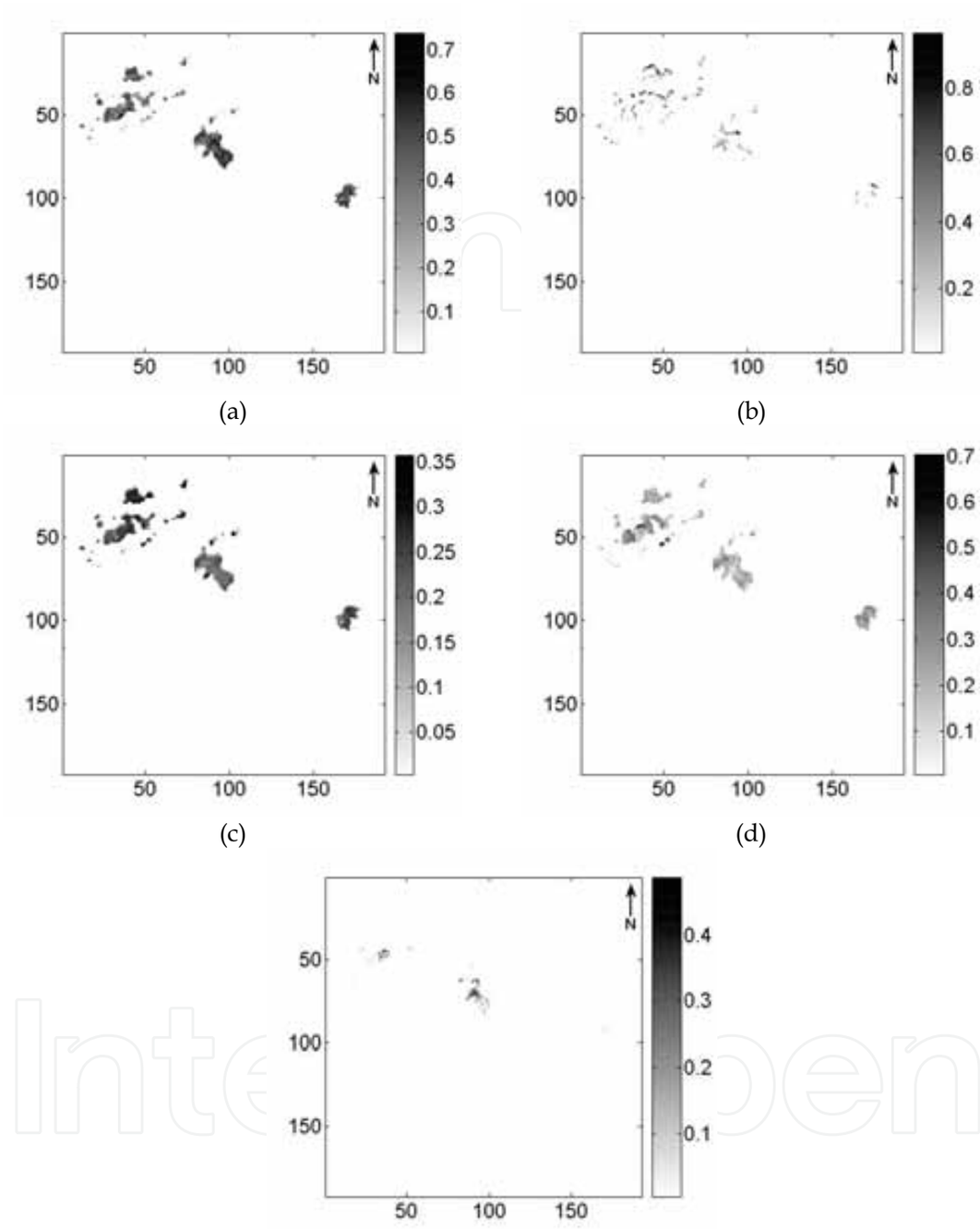

Fig. 5. Detailed classification: Endmember fraction maps (196*196 pixels) derived from Hybrid constrained linear unmixing: (a) calcite, (b) clays (kaolinite and illite), (c) gypsum, (d) oxides (hematite and goethite) and (e) pyrite.

calcimetry, X-ray diffraction and polished section analysis. Tailing samples were collected from deposit location areas (considered as pollution source). Mineral library spectra (Grove, 1992) were resampled to hybrid band passes before classification. 96 % of the classified pixels show an error lower than $1.9\ 10^{-5}$. This classification is then acceptable. The resulting endmember fraction maps show an interesting contribution of the hybrid image for mineral detection.

The results of linear constrained spectral unmixing show different fraction maps (Figure 5), which show the comparison of the variability's of the endmember distribution in a spatial context. Among the 5 endmembers, only calcite and gypsum are of most interest. Indeed, this is not a surprising result since the magazine rocks are carbonates. The unmixing images suggest a relative significant concentration of Hematite mineral within the tailing deposit area (resulting from pyrite oxidizing exposure surfaces) and in the soils (polluted soils by alluvium) (due to the lithologic nature of soils and the eroded tailings). This result can explain the reddish color of deposit area and soils. The clays fraction map shows also a less significant concentration within deposit than in the soils (polluted soils by alluvium). For pyrite concentration, is more detected within deposit, particularly in Bouaouane dykes, than soils. This would suggest that this mineral is almost completely oxidized in the deposit surface which is exposed to the climatic effects. It is presence in the soils (polluted soils by alluvium), can be explicated by the wind and hydrous erosion effects which transport and depose tailings far from deposit.

4. Results analysis and discussion

In this section, we compare the abundance of minerals considered by both multi-scale methods. Indeed, the results of hybrid classification are then compared to the abundances of minerals (endmembers) calculated from laboratory analysis. This comparison allowed validating the results of the adopted tailing cartography approach. The statistical regression analysis consists on calculation of the coefficient of determination (R^2). The analysis was conducted for the whole samples.

The comparison was revealed the existence of positive linear regression with variable intensities. According to the results obtained and exposed in the figure 6, we note, that the coefficient of determination is 0.85 (figure 6 b) for clay minerals. The slope of the regression equation is near unity (0.98), and the intercept is 1.14. This indicates that the hybrid image data can well quantify the abundance of clays. For pyrite, the coefficient of determination is also important (0.62) (figure 6 e). The slope of the regression equation is 0.77 and the intercept is 0.7. The pyrite can be quantified by hybrid image. For gypsum, the coefficient of regression is also important (0.6) (figure 6 c). However, the slope of the regression equation is weak (0.19) and the intercept close to 0 (0.06). The abundances estimated by laboratory analysis are not equal to those quantified by hybrid image, and thus the regression slope does not approach a value of 1. For oxyhydroxides, the coefficient of determination is also above 0.5 (0.506) (figure 6 d). The slope of the regression equation is 0.67 and the intercept close to 0 (0.07). This indicates that hybrid image can quantify relatively hematite and goethite. For calcite, the coefficient of determination is 0.504 (figure 6 a). The slope of the regression equation is 0.73 and the intercept is 52. This raised value of the intercept is probably due to underestimation of the abundance from hybrid image. Furthermore, the

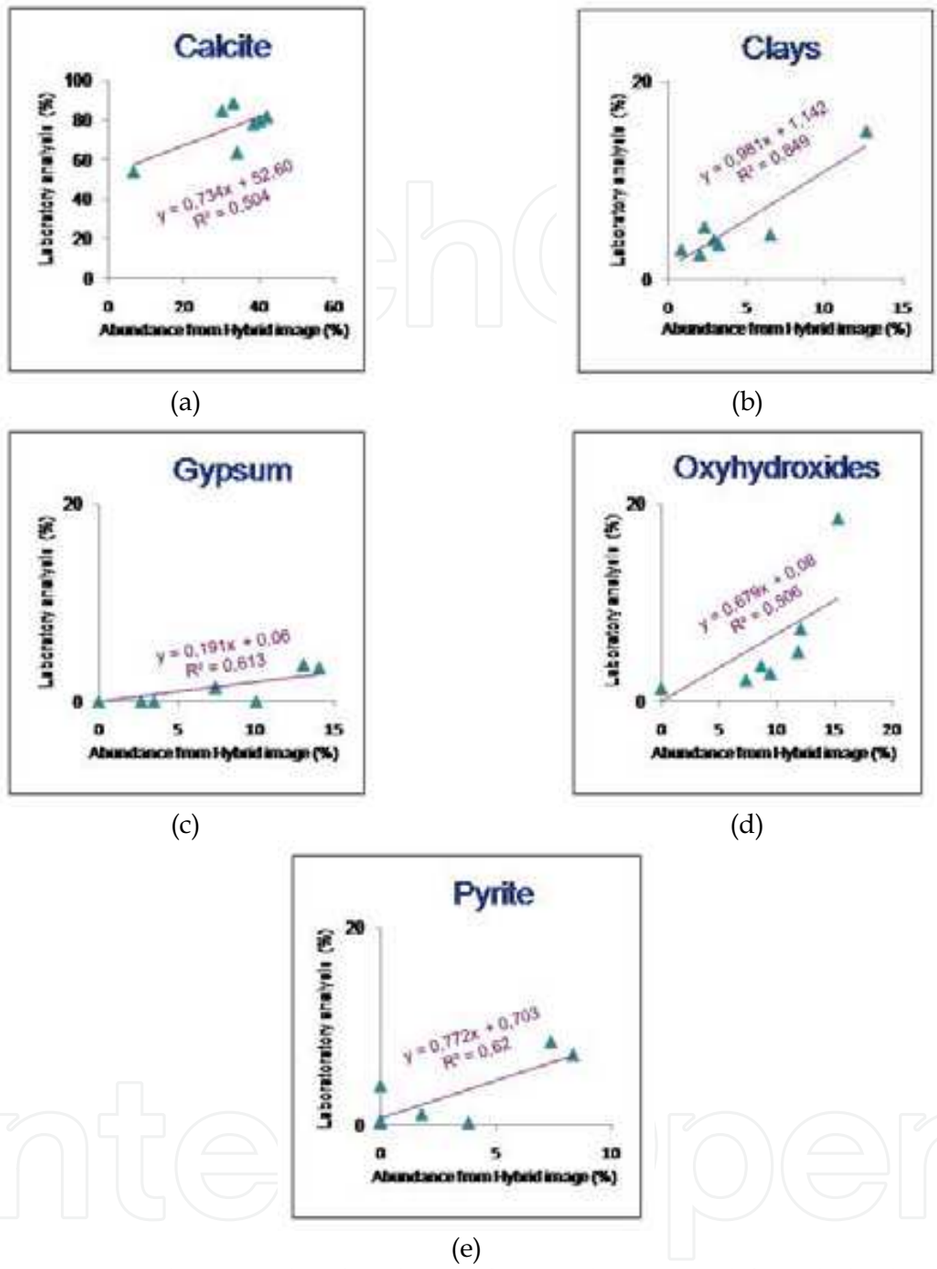

Fig. 6. Comparison between the abundance of minerals estimated from hybrid unmixing results and the laboratory analysis results.

values of R2 showed that the regression for particularly clays and pyrite had the higher goodness of fit than those for calcite, gypsum and oxyhydroxides .

The above results of regression analysis imply that positive attitudes are related to concrete complementarities of hybrid unmixing and laboratory analysis results. The experiment was

conducted only for the relatively few used samples. Thus, we should note that there is a limit for a rigorous interpretation of the regression results.

4. Conclusion

In this chapter we have described a tailing cartography approach which is very useful in the case of multispectral multisensory study. A simplified version of the Multisensor Multiresolution Technique (MMT) for image fusion was also presented. Moreover, we have tested this technique on two different multispectral sensors; Landsat MS/Pan image and ASTER SWIR image. The unmixing results' has shown that the hybrid multispectral data can be used successfully to provide information on refining mine tailing cartography. Furthermore, multispectral hybrid image shows a complementary result with laboratory analysis for selected endmember minerals.

The classification of hybrid multispectral data which is based on the constrained linear spectral unmixing using JPL mineral library spectra generated mineral detailed maps. Only mine tailing pixels were used in the analysis. In fact, the first coarse classification was used to highlight the mine tailing area and masking the surrounding zone in the hybrid image. The mask was validated with high resolution image before being used in the classification process.

The resulting mineral fraction maps show the comparison of the variability of their distribution in a spatial context for classification method. These results show an interesting contribution of the hybrid image for mineral detection. Furthermore, multispectral hybrid image classification shows complementary results with laboratory analysis, used as field truth, for selected endmember minerals.

Furthermore, future refinement of the detailed tailing maps will result in presence of high spectral and spatial resolution data. Moreover, we propose a strict sampling in the mine tailing deposit for more significant mineralogy quantification.

5. Acknowledgments

The authors would like to thank the NASA Land Processes Distributed Active Archive Center and the User Services USGS Earth Resources Observation and Science (EROS) for providing numerous remotely sensed data.

6. References

Boardman, J. W. (1993). Automatic spectral unmixing of AVIRIS data using convex geometry concepts, *Summaries 4th Annual JPL Airborne Geoscience Workshop*, October 25-29, Vol. 1 AVIRIS Workshop.

Carreiras, J. M. B.; Shimabukuro, Y. E. & Pereira, J. M. C. (2002). Fraction images derived from SPOT-4 VEGETATION data to asses land-cover change over the State of Mato Grosso, Brazil*, Int. J. Remote Sens.*, vol 23, n°. 23, pp. 4979-4983.

Chavez, P. S.; Sides, S. C. & Anderson, J. A. (1991). Comparaison of three different methods to merge multiresolution and multispectral data: Landsat TM and SPOT panchromatic, *Photogramm. Eng. Remote Sensing*, vol. 57, N° 3.

Cooley, T.G.; Anderson, P.; Felde, G.W.; Hoke, M.L.; Ratkowski, A.J.; Chetwynd, J.H.; Gardner, J.A.; Adler-Golden, S.M.; Matthew, M.W.; Berk, A.; Bernstein, L.S.; Acharya, P.K. & Miller, D. (2002). FLAASH, a MODTRAN4-based atmospheric correction algorithm, its application and validation, *International Geosciences and Remote Sensing Symposium IGARSS'02*, vol.3, 2002, pp. 1414 -1418.

Grove, C. I., Hook, S. J., and Paylor II, E. D. (1992). Laboratory Reflectance Spectra of 160 Minerals, 0.4 to 2.5 Micrometers, *Jet Propulsion Laboratory Publication 92-2*.

Haertel, V. F. & Shimabukuro Y. E. (2005). Spectral linear mixing model in low spatial resolution image data, *IEEE Trans. Geosci. Remote Sensing*, vol. 43, N° 11.

Hu, Y. H.; Lee, H. B.; & Scarpace, F. L. (1999). Optimal linear spectral unmixing, *IEEE Trans. Geosci. Remote Sens.*, vol. 37, N°. 1, 1999, pp. 639-644.

Keshava, N. & Mustard, J. F. (2002). Spectral unmixing, *IEEE Signal Process. Mag.*, vol. 19, N°. 1, 2002, pp. 44-57.

Mansouri, A. (1980). Gisements de Pb-Zn et Karstification en milieu continental: le district du Jbel Hallouf- Sidi Bou Aouane (Tunisie Septentrionale), Thèse de doctorat, *Univ. de Pierre et Marie Curie, Paris VI*, 199 p.

Matlab (2004). MATLAB Users Guide, *MATLAB 7.0 Release 14*.

Mezned, N.; Abdeljaouad, S. & Boussema, M.R. (2007). Unmixing Based Landsat ETM+ and ASTER Image Fusion for Hybrid Multispectral Image Analysis, *IEEE International on Geoscience and Remote Sensing Symposium IGARSS'07*.

Peters, D. C., and Hauff, P. L. (2000). Multispectral remote sensing to characterize mine waste, *Springer-Verlag*, Berlin, pp. 113-164.

Richards, J. A. (1986). Remote sensing digital image analyzes. An introduction, Berlin, Germany. *Springer-Verlag*.

Shimabukuro, Y. E., and Smith, J. A. (1991). The least-squares mixing models to generate fraction images derived from remote sensing multispectral data, *IEEE Trans. Geosci. Remote Sens.*, vol. 29, n°. 1, pp. 16-20.

Singer, (1981). Near-infrared spectral reflectance of mineral mixtures: systematic combinations of pyroxenes, olivine, and iron oxides. *Journal of geophysical Research*, 86, pp. 7967-7982.

Souissi, F. (2007). Minéralogie et géochimie des gîtes minéraux, des séries sédimentaires anciennes et de l'environnement (Synthèse des travaux de recherche). Habilitation universitaire, Faculté des Sciences de Tunis *FST*, 83p.

Zhukov, B.; Oertel, D.; Lanzi, F. & Reinhäckel G. (1999). Unmixing-Based Multisensor Multiresolution Image Fusion, *IEEE Trans. Geosci. Remote Sensing*, vol. 37, N° 3.

Zurita Milla, R.; Clevers, J.G.P.W. and Schaepman. M.E. (2008). Unmixing-based Landsat TM and MERIS FR data fusion, *IEEE Geoscience and Remote Sensing Letters 5*, pp. 453-457.

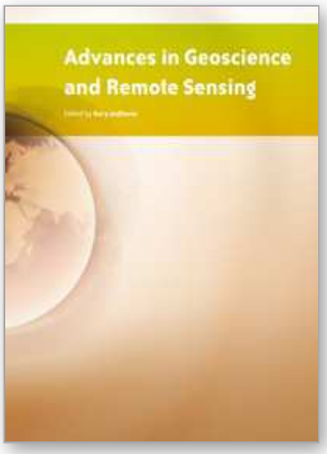

Advances in Geoscience and Remote Sensing

Edited by Gary Jedlovec

ISBN 978-953-307-005-6

Hard cover, 742 pages

Publisher InTech

Published online 01, October, 2009

Published in print edition October, 2009

Remote sensing is the acquisition of information of an object or phenomenon, by the use of either recording or real-time sensing device(s), that is not in physical or intimate contact with the object (such as by way of aircraft, spacecraft, satellite, buoy, or ship). In practice, remote sensing is the stand-off collection through the use of a variety of devices for gathering information on a given object or area. Human existence is dependent on our ability to understand, utilize, manage and maintain the environment we live in - Geoscience is the science that seeks to achieve these goals. This book is a collection of contributions from world-class scientists, engineers and educators engaged in the fields of geoscience and remote sensing.

InTech Europe
University Campus STeP Ri
Slavka Krautzeka 83/A
51000 Rijeka, Croatia
Phone: +385 (51) 770 447
Fax: +385 (51) 686 166
www.intechopen.com

InTech China
Unit 405, Office Block, Hotel Equatorial Shanghai
No.65, Yan An Road (West), Shanghai, 200040, China
中国上海市延安西路65号上海国际贵都大饭店办公楼405单元
Phone: +86-21-62489820
Fax: +86-21-62489821

IntechOpen